Contents lists available at ScienceDirect

Journal of Contaminant Hydrology

journal homepage: www.elsevier.com/locate/jconhyd

Analytic solutions for colloid transport with time- and depth-dependent retention in porous media

Feike J. Leij [a,*], Scott A. Bradford [b], Antonella Sciortino [a]

[a] Department of Civil Engineering and Construction Engineering Management, California State University, 1250 Bellflower Boulevard, Long Beach, CA 90840, United States
[b] US Salinity Laboratory USDA, ARS, 450 W. Big Springs Road, Riverside, CA 92507-4617, United States

ARTICLE INFO

Article history:
Received 15 June 2016
Received in revised form 4 October 2016
Accepted 31 October 2016
Available online 1 November 2016

ABSTRACT

Elucidating and quantifying the transport of industrial nanoparticles (e.g. silver, carbon nanotubes, and graphene oxide) and other colloid-size particles such as viruses and bacteria is important to safeguard and manage the quality of the subsurface environment. Analytic solutions were derived for aqueous and solid phase colloid concentrations in a porous medium where colloids were subject to advective transport and reversible time and/or depth-dependent retention. Time-dependent blocking and ripening retention were described using a Langmuir-type equation with a rate coefficient that respectively decreased and increased linearly with the retained concentration. Depth-dependent retention was described using a rate coefficient that is a power-law function of distance. The stream tube modeling concept was employed to extend these analytic solutions to transport scenarios with two different partitioning processes (i.e., two types of retention sites). The sensitivity of concentrations was illustrated for the various time- and/or depth-dependent retention model parameters. The developed analytical models were subsequently used to describe breakthrough curves and, in some cases, retention profiles from several published column studies that employed nanoparticle or pathogenic microorganisms. Simulations results provided valuable insights on causes for many observed complexities associated with colloid transport and retention, including: increasing or decreasing effluent concentrations with continued colloid application, delayed breakthrough, low concentration tailing, and retention profiles that are hyper-exponential, exponential, linear, or non-monotonic with distance.

1. Introduction

Knowledge of the transport and fate of natural colloids such as microbes, clay minerals, rock fragments, and organic debris as well as engineered nanoparticles such as silver, zinc, and graphene oxides, silicon, and lead sulfide is important. The presence of colloids in solution is undesirable if groundwater is to be used as drinking water by humans or livestock. For example, pathogenic microbes and engineered nanoparticles can directly pose a threat for human health (Gerba and Smith, 2005; Boxall et al., 2007), while colloid-size particles may facilitate the movement of low-solubility toxic contaminants (Sen and Khilar, 2006). Colloids may also affect the hydraulic properties of the subsurface by altering the pore structure to produce clogging (Torkzaban et al., 2015).

Mathematical models are commonly used to elucidate and quantify colloid transport and retention processes that are studied in packed column experiments under steady-steady water flow and solution chemistry conditions. These models typically solve the advection-dispersion equation that includes a model for colloid partitioning between the aqueous and solid phases of the porous medium (Wang et al., 2013; Neukum et al., 2014; Bradford et al., 2011). Values for dispersivity, which may be approximated from independent displacement experiments using ionic or other tracers, are typically low. The focus of this work is on analytical solutions for aqueous and solid phase colloid concentrations resulting from advective transport for a variety of partitioning models. Analytical solutions, which are typically derived for well-defined and simplified conditions, may serve an important role to: analyze results from experimental studies, illustrate the importance of model parameters, verify numerical model results, and conveniently simulate transport behavior at larger temporal and/or spatial scales (Javandel et al., 1984; Vanderborght et al., 2005).

The colloid partitioning process is very sensitive to the solution chemistry, hydrodynamic conditions, particle size distribution of colloid and porous medium, and physical and chemical heterogeneity of the colloid and porous medium surfaces (Sen and Khilar, 2006; Sasidharan et al., 2014; Bradford and Torkzaban, 2015). Although colloid retention has often been assumed to be irreversible

* Corresponding author.
E-mail addresses: feike.leij@csulb.edu (F.J. Leij), Scott.Bradford@ars.usda.gov (S.A. Bradford), antonella.sciortino@csulb.edu (A. Sciortino).

http://dx.doi.org/10.1016/j.jconhyd.2016.10.006
0169-7722/

(Yao et al., 1971), low levels of colloid release frequently occur when attraction of colloids to the solid phase is relatively weak (Ryan and Elimelech, 1996). Consequently, partitioning models should allow for release of colloids from the solid phase. The following four models will be used in this study to describe colloid transport: (1) first-order kinetics, (2) time-dependent blocking of retention sites; (3) time-dependent ripening of retention sites; and (4) depth-dependent retention.

The first model considers first-order kinetics where colloid partitioning is proportional to the difference in aqueous and solid concentrations (e.g., Harvey and Garabedian, 1991). This type of equation is mathematically convenient and arises as a limiting case of some of more complex partitioning models presented in the following. It has been widely used to describe the adsorption of cations and anions by the soil solid phase (Lapidus and Amundson, 1952; Sposito, 1989).

The second model considers time-dependent blocking of retention sites. Blocking is reflected by a decrease in the retention rate coefficient during filling of a finite number of retention sites (Chowdhury et al., 2011; Liang et al., 2013). This site blocking effect has been described using a Langmuir-type model (Camesano et al., 1999; Deshpande and Shonnard, 1999; Yuan and Shapiro, 2012; Neukum et al., 2014). This type of problem has long been studied for chemical transport in packed columns. Bohart and Adam (1920) first provided an analytical solution for advective transport of chlorine gas in a charcoal bed with irreversible Langmuirian sorption. Leij et al. (2015) presented an alternative procedure to solve the same problem for colloid transport. Thomas (1944, 1948) published an analytical solution for reversible ion exchange described with a Langmuir isotherm during flow in a zeolite column. This model has been widely applied in chemical and environmental engineering (e.g., Hiester and Vermeulen, 1952; Vijayaraghavan and Yun, 2008; Mao et al., 2015). In this work, a simpler solution procedure is presented that is based on variable and Laplace transformations.

The third model attempts to describe partitioning for time-dependent "ripening" of the solid phase, which results in an increase in the colloid retention rate coefficient. This occurs when retained colloids act as favorable sites for subsequent retention (Deshpande and Shonnard, 1999; Bradford et al., 2013). The partitioning model for ripening is very similar to that for blocking and analytical solutions of the resulting nonlinear problem may be obtained by adapting expressions for aqueous and solid concentrations for blocking.

The fourth model assumes depth- or position-dependent partitioning. In column experiments the retained colloid concentration frequently does not follow an exponential decrease with distance as predicted by the first-order model (Bradford et al., 2013). Rather, retention profiles sometimes exhibit a hyperexponential shape, with greater amounts of retention near the column inlet and less away from it. Hyperexponential retention profiles have been attributed to straining (Bradford et al., 2003), heterogeneity of the charge and/or size of the colloid population (Li et al., 2004; Tong et al., 2005), heterogeneity of the solid surface of the medium (Tufenkji and Elimelech, 2005), and system hydrodynamics (Bradford et al., 2011). Bradford et al. (2003) proposed an empirical retention rate coefficient using a power law function of distance. The analytic solution for this fourth model is presented in order to quantify a decrease in the retention rate coefficient with travel distance in porous media.

The kinetics of colloid retention may frequently not be described with a single partitioning model (Bradford et al., 2013). This study therefore also considers the possibility of bimodal partitioning where the porous medium has two types of kinetic sites with a different retention rate. Colloid transport is then modeled by determining the total aqueous and solid or retained concentrations as the weighted sum of the concentrations obtained for unimodal partitioning.

The objectives of this study are as follows: (1) derive analytical solutions for the aqueous and solid phase colloid concentrations for four partitioning models, (2) illustrate the effect of the partitioning model on spatial and temporal colloid profiles, and (3) describe results from laboratory studies with the analytical solutions for aqueous and solid concentrations and estimate model parameters.

2. Mathematical

The mass balance equation for colloid transport involving advection and retention during one-dimensional steady water flow in a porous medium with a uniform water content is given as:

$$\frac{\partial C}{\partial t}+\frac{\partial Q}{\partial t}+V\frac{\partial C}{\partial z}=0 \qquad z>0 \quad , \quad t>z/V \tag{1}$$

where C is the aqueous colloid concentration, Q is the solid concentration expressed as amount of retained colloids per volume of aqueous phase, t is time, z is distance from the inlet, and V is the pore-water velocity. Note that $Q=\rho S/\theta$ where S is the solid phase colloid concentration, expressed as amount of retained colloid per mass of soil, ρ is the soil bulk density, and θ is the volumetric water content. If a pulse with a uniform colloid concentration is supplied at the inlet of, for example, a sand column that is initially free of colloid, the boundary and initial conditions can be given as:

$$C(0,t)=C_oH(t_o-t), C(z,0)=Q(z,0)=0 \tag{2a, b}$$

where t_o is the time that colloid is applied at the column inlet (pulse duration), and H is the Heaviside or unit-step function. The complete mathematical problem requires an expression for the retention rate in Eq. (1). Solutions for the aqueous and solid concentrations will be provided in the following for four different partitioning models.

2.1. First-order retention and release

The classical first-order rate equation for retention and release is given by:

$$\frac{\partial Q}{\partial t}=k_aC-k_dQ \tag{3}$$

where k_a is the "clean-bed" first-order retention or attachment coefficient and k_d is the release or detachment coefficient. Solving Eqs. (1)–(3) is straightforward (cf. Leij and Sciortino, 2012) and yields the expressions:

$$C(z,t)=H\left(t-\frac{z}{V}\right)C_o\left[J\left(\frac{k_a z}{V},k_d\left(t-\frac{z}{V}\right)\right)-H\left(t-t_o-\frac{z}{V}\right)J\left(\frac{k_a z}{V},k_d\left(t-t_o-\frac{z}{V}\right)\right)\right] \tag{4}$$

$$Q(z,t)=\frac{k_a C_o}{k_d}\left[H\left(t-\frac{z}{V}\right)\left(1\text{-}J\left(k_d\left(t-\frac{z}{V}\right),\frac{k_a z}{V}\right)\right)-H\left(t-t_o-\frac{z}{V}\right)\left(1\text{-}J\left(k_d\left(t-t_o-\frac{z}{V}\right),\frac{k_a z}{V}\right)\right)\right] \tag{5}$$

where the *J*-function by Goldstein (1953) is defined by Eqs. (A15a) and (A15b).

2.2. Blocking

Blocking of colloid retention is modeled using the following Langmuirian type of equation (Adamczyk et al., 1994; Wang et al., 2013) as:

$$\frac{\partial Q}{\partial t}=\left(1-\frac{Q}{Q_m}\right)k_a C-k_d Q \tag{6}$$

where Q_m is the upper limit of the solid concentration expressed as maximum amount of retained colloids per volume of aqueous phase. Eq. (6) implies that the filling of retention sites is a second-order process. If there is no blocking ($Q_m\to\infty$), then Eq. (6) becomes the common first-order rate equation given in Eq. (3). The simpler irreversible model by Bohart and Adam (1920) is obtained when $k_d\to 0$.

Thomas (1944) provided a well-known solution for reversible exchange for a fixed influent concentration (step input). The nonlinear problem was transformed to a linear hyperbolic differential equation that was solved with the help of the Riemann method. The solutions for the aqueous and solid concentrations were expressed in terms of the zero-order modified Bessel function. A similar problem of transport without dispersion and for a Dirac-type inlet concentration was considered by Wade et al. (1987) based on the procedure by Thomas (1944) using a double Laplace transformation. Appendix A outlines a more convenient alternative solution procedure for a pulse-type application, which can be modified for other influent profiles. The following expressions may be obtained for the aqueous and solid phase concentrations:

$$C(z,t)=\frac{C_o}{u(z,t)}\times\begin{cases}\exp\left(\frac{\alpha z}{V}+\beta\left(t-\frac{z}{V}\right)\right)-\Gamma\left(\frac{\alpha z}{V},\beta\left(t-\frac{z}{V}\right)\right) & t_o>t-z/V\\ \exp(\beta t_o)\Gamma\left(\frac{\alpha z}{V},\beta\left(t-t_o-\frac{z}{V}\right)\right)-\Gamma\left(\frac{\alpha z}{V},\beta\left(t-\frac{z}{V}\right)\right) & t_o<t-z/V\end{cases} \tag{7}$$

$$Q(z,t)=\frac{k_a C_o}{\beta u(z,t)}\times\begin{cases}\exp\left(\frac{\alpha z}{V}+\beta\left(t-\frac{z}{V}\right)\right)-\Gamma\left(\frac{\alpha z}{V},\beta\left(t-\frac{z}{V}\right)\right)-I_0\left(2\sqrt{k_a k_d\frac{z}{V}\left(t-\frac{z}{V}\right)}\right) & t_o>t-z/V\\ \exp(\beta t_o)\left[\Gamma\left(\frac{\alpha z}{V},\beta\left(t-t_o-\frac{z}{V}\right)\right)+I_0\left(2\sqrt{k_a k_d\frac{z}{V}\left(t-t_o-\frac{z}{V}\right)}\right)\right]+ & \\ \quad-\Gamma\left(\frac{\alpha z}{V},\beta\left(t-\frac{z}{V}\right)\right)-I_0\left(2\sqrt{k_a k_d\frac{z}{V}\left(t-\frac{z}{V}\right)}\right) & t_o<t-z/V\end{cases} \tag{8}$$

where $u(z,t)$ is given by:

$$u(z,t)=\begin{cases}\exp\left(\frac{\alpha z}{V}+\beta\left(t-\frac{z}{V}\right)\right)-\Gamma\left(\frac{\alpha z}{V},\beta\left(t-\frac{z}{V}\right)\right)+\Gamma\left(\frac{k_a z}{V},k_d\left(t-\frac{z}{V}\right)\right) & t_o>t-z/V\\ \exp(\beta t_o)\left[\Gamma\left(\frac{\alpha z}{V},\beta\left(t-t_o-\frac{z}{V}\right)\right)-\Gamma\left(\frac{k_a z}{V},k_d\left(t-t_o-\frac{z}{V}\right)\right)\right]-\Gamma\left(\frac{\alpha z}{V},\beta\left(t-\frac{z}{V}\right)\right)+ & \\ \quad+\Gamma\left(\frac{k_a z}{V},k_d\left(t-\frac{z}{V}\right)\right)+\exp\left(\frac{k_a z}{V}+k_d\left(t-\frac{z}{V}\right)+\gamma t_o\right) & t_o<t-z/V\end{cases} \tag{9}$$

with I_0 as the zero-order modified Bessel function of the first kind and the auxiliary function Γ, which is related to the *J*-function by Goldstein (1953), is defined as:

$$\Gamma(a,b)=\int_0^a\exp(a-\lambda)I_0\left(2\sqrt{\lambda b}\right)d\lambda \tag{10}$$

Furthermore:

$$\alpha=\frac{k_a k_d Q_m}{k_a C_o+k_d Q_m}\quad,\quad\beta=k_a k_d/\alpha\quad,\quad\gamma=\frac{k_a C_o}{Q_m} \tag{11a, b, c}$$

In the absence of colloid release by the medium (i.e., $k_d=0$) the above solution for reversible retention lead to the simpler irreversible solution (Leij et al., 2015). Comparisons between the two models have been made by many authors (e.g., Vijayaraghavan and Yun, 2008; Chu, 2010).

2.3. Ripening

A simple model for ripening assumes a linear increase in the retention rate with Q given as (cf. Yuan and Shapiro, 2012; Hosseini and Tosco, 2013):

$$\frac{\partial Q}{\partial t} = (1 + rQ)k_a C - k_d Q \quad (k_d \neq k_a r C_o) \tag{12}$$

where r is an empirical parameter, expressed as volume of aqueous phase per amount of retained colloids. Higher values for r reflect a greater degree of ripening. The previous solution for Langmuirian blocking can also be used for the linear ripening model by replacing Q_m with $-1/r$ in Eqs. (7)–(11). For negligible release, the solution for irreversible blocking can be used by again setting $Q_m = -1/r$.

2.4. Depth-dependent retention

A simple empirical approach to account for hyperexponential retention profiles is to make the retention rate coefficient a power law function of depth or distance from the inlet (Bradford et al., 2003):

$$\frac{\partial Q}{\partial t} = \left(1 + \frac{z}{d_{50}}\right)^n k_a C - k_d Q \tag{13}$$

where d_{50} is the median particle-size of the porous medium, and n is a negative-valued empirical exponent. Appendix B outlines a simple solution procedure for this problem for a pulse-type application based on Laplace transformation. The following expressions were obtained for the aqueous and solid phase concentrations:

$$C(z,t) = H\left(t - \frac{z}{V}\right) C_o \left[J\left(A, k_d\left(t - \frac{z}{V}\right)\right) - H\left(t - t_o - \frac{z}{V}\right) J\left(A, k_d\left(t - t_o - \frac{z}{V}\right)\right)\right] \tag{14}$$

$$Q(z,t) = \frac{k_a C_o}{k_d}\left(1 + \frac{z}{d_{50}}\right)^n \left[H\left(t_o + \frac{z}{V} - t\right) + H\left(t - t_o - \frac{z}{V}\right) J\left(k_d\left(t - \frac{z}{V}\right), A\right) - J\left(k_d\left(t - t_o - \frac{z}{V}\right), A\right)\right] \tag{15}$$

where:

$$A = \frac{d_{50} k_a}{(1+n)V}\left[\left(1 + \frac{z}{d_{50}}\right)^{1+n} - 1\right] \tag{16}$$

with J again as Goldstein's function (cf. Eq. (A15)).

2.5. Two-site model

Two different retention mechanisms are used in the bimodal partitioning model. The bimodal model assumes that $Q = Q_1 + Q_2$ in Eq. (1), where the subscripts 1 and 2 refer to type-1 and type-2 sites. It is assumed that a fraction f of the colloids, which reside in "subdomain 1" of the porous medium, is controlled by a particular partitioning mechanism while another mechanism is used to describe partitioning for the remaining colloids residing in "subdomain 2." A solution for colloid transport in the entire domain is obtained as the weighted sum of the unimodal solutions:

$$C = f C_1^{uni} + (1-f) C_2^{uni}, Q = f Q_1^{uni} + (1-f) Q_2^{uni} \tag{17a, b}$$

where the superscript "uni" refers to the scenario were all retentions sites are either of type 1 or 2. The solution hinges on the validity of the "streamtube" concept, i.e., colloid transport in either of the two subdomains is not affected by the other subdomain, and the superposition of one or two nonlinear solutions.

3. Examples

3.1. Blocking

Blocking of retention sites will result in lower retention and greater colloid transport through the aqueous phase. Limitation of available retention sites is determined by the actual and maximum solid concentrations Q and Q_m. The former is affected by the aqueous concentration as well as by retention and release coefficients. A large number of potential retention sites (Q_m) may mitigate the effect of blocking. Fig. 1 shows aqueous and solid concentration versus depth 20 min after the application of a 10-min pulse with an input concentration C_o. Three different values of Q_m were used. The lowest Q_m produces a relatively rapid increase in the aqueous concentration ($10 < z < 20$ cm) because of the limited opportunity for retention due to blocking, which is also demonstrated by the low values for the solid concentration Q/C_o. If blocking is less pronounced, there is more opportunity for retention ($0 < z < 10$) and less colloid will remain in the original pulse traveling through the medium ($10 < z < 20$). Retained colloids will eventually appear in the effluent because of release.

Fig. 2 illustrates the effect of the release coefficients k_d for pulse application to a 20-cm column with reversible blocking. After the pulse has moved through the column the aqueous concentration immediately becomes zero for $k_d = 0$ because no colloid is released back into the aqueous phase. Increasing the value of k_d produces greater amounts of colloid release and a corresponding higher aqueous concentration at the pulse location, i.e., between 10- and 20-cm-depth. The influence of k_d on Q becomes most apparent for $x < 10$ cm. In particular, the value of Q at the inlet rapidly decreases with increasing k_d because of release. Consequently, reversible blocking produces nonmonotonic retention

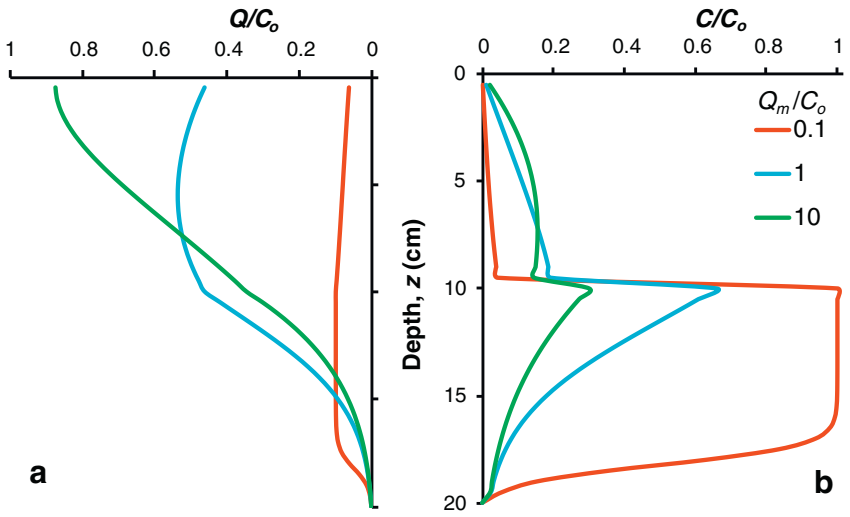

Fig. 1. Normalized solid (Q/C_o; Panel a) and aqueous (C/C_o; Panel b) phase concentrations versus depth at $t = 20$ min according to the blocking model for a pulse input with $t_o = 10$ min, $V = 1$ cm/min, $k_a = 0.2$ min^{-1}, $k_d = 0.05$ min^{-1}, and $Q_m/C_o = 0.1$, 1, and 10.

profiles. The phenomenon that the maximum solid concentration occurs after the colloid pulse has passed in the aqueous phase has been observed by Bradford et al. (2006), Tong et al. (2005), and Liang et al. (2013).

Fig. 3 shows concentrations profiles, 20 min after application commenced, for retention rates $k_a = 0.1$, 0.2 and 0.4 min^{-1}. The retention rate k_a has an opposite impact on the solid and aqueous concentrations than k_d. For the larger rate of 0.4 min^{-1} more colloids are retained near the inlet, which results in a lower aqueous concentration at the location of the pulse ($10 < z < 20$ cm). Blocking and retention lead to more pronounced differences in Q for $z < 10$ cm and in C for $z > 10$ cm.

3.2. Ripening

In the ripening model the coefficient r enhances retention at greater solid concentrations. Fig. 4 displays solid and aqueous concentrations for three r–values for irreversible retention ($k_d = 0$). The ripening causes an increase in available retention sites when the solid concentration increases. In the aqueous phase colloid only occurs at the location of the pulse ($5 < z < 15$ cm) because there is no dispersion or release. For more ripening ($r = 5$ and 10), the concentration actually increases with depth in this region because for shorter times (smaller depths) the increased retention due to ripening may reduce the aqueous concentration. Ripening produces hyperexponential retention profiles, with the solid phase concentration highest near the inlet ($z = 0$), because the retention capacity increases with time and in this example retention was irreversible.

3.3. Depth-dependent retention

In addition to k_a, Eq. (13) indicates that the amount of retention is controlled by parameters n and d_{50} in the depth-dependent retention model. The effect of parameters n and d_{50} on depth-dependent partitioning is illustrated for continuous colloid application at the inlet in Figs. 5 and 6, respectively. A step input is used to show the increase in colloid retention near the inlet more clearly. The concentration profiles in Fig. 5 are obtained for the exponent n equal to -0.1, -0.3, and -0.9 while setting $d_{50} = 0.02$ cm. For all three n-values, the solid

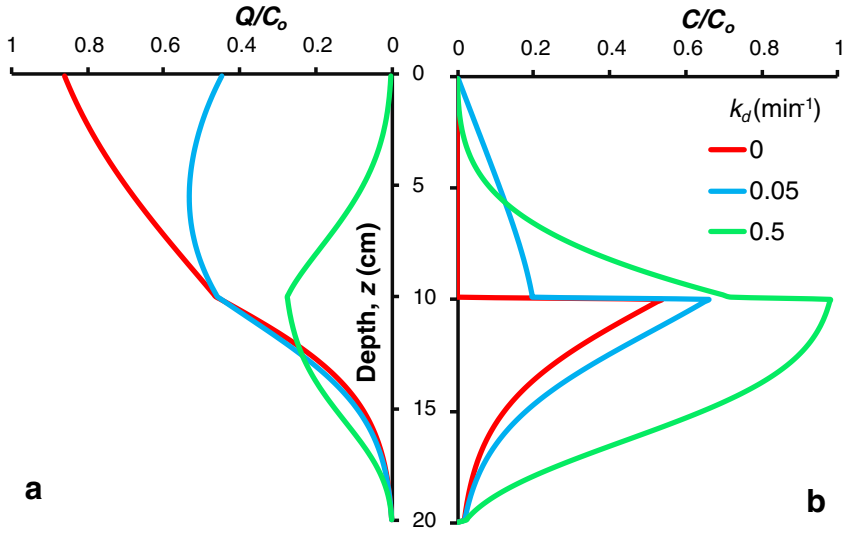

Fig. 2. Normalized solid (Q/C_o; Panel a) and aqueous (C/C_o; Panel b) phase concentrations versus depth at $t = 20$ min according to the blocking model for a pulse input with $t_o = 10$ min, $V = 1$ cm/min, $Q_m/C_o = 1$, $k_a = 0.2$ min^{-1}, and $k_d = 0$, 0.05 or 0.5 min^{-1}.

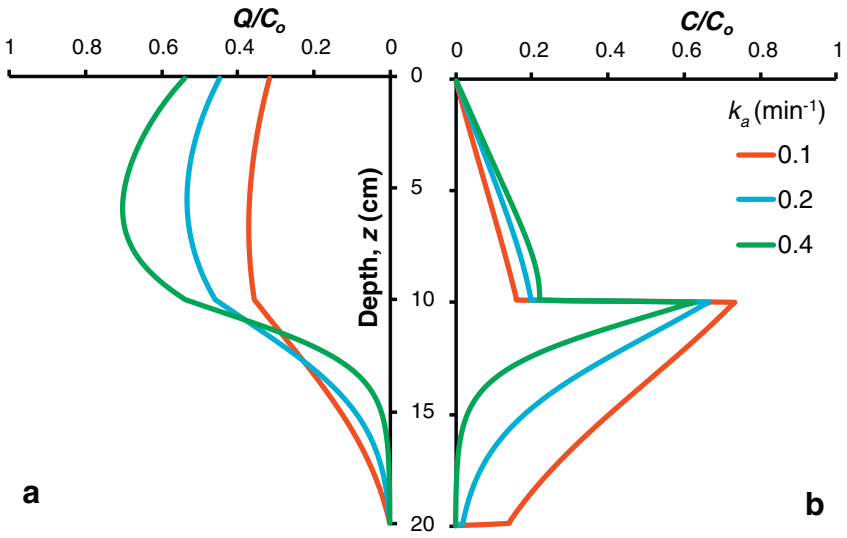

Fig. 3. Normalized solid (Q/C_o; Panel a) and aqueous (C/C_o; Panel b) phase concentrations versus depth at $t = 20$ min according to the blocking model for a pulse input with $C_o = 1$ cm^{-3}, $t_o = 10$ min, $V = 1$ cm/min, $Q_m = 1$ cm^{-3}, $k_d = 0.05$, and $k_a = 0.1$, 0.2 or 0.4 min^{-1}.

concentration decreases rapidly in a nonlinear fashion with depth while a more linear behavior occurs for the aqueous concentration. The greatest solid and lowest aqueous concentration occurs for the most negative n of −0.9. The role of the "median particle diameter" d_{50} is examined in Fig. 6 where n is set equal to −0.3. The shape of the concentration profiles is similar for all three d_{50}. The smaller d_{50} results in a reduced opportunity for retention and a commensurate greater aqueous concentration.

3.4. Two-site model

As an illustration of the two-side model consider blocking where retention for part of the sites is reversible and irreversible for the remaining sites. The breakthrough curves for five different fractions f of reversible sites are shown in Fig. 7a. A greater f results in more colloid breakthrough. Fig. 7b shows the retained profile, the effect of f becomes pronounced after the pulse has passed ($0 < z < 10$ cm). Note that the retention profiles become nonmonotonic in shape with increasing f (number of reversible sites).

4. Applications

This section discusses the application of the analytical solutions to describe datasets of colloid breakthrough curves and, in some instance, retention profiles published by Kim et al. (2010), Kasel et al. (2013), Wang et al. (2013), and Sasidharan et al. (2014). Table 1 summarizes experimental information such as colloid type, pore-water velocity V, duration of pulse and experiment t_o and t_{exp}, column length L, water content θ, and breakthrough curve (BTC) or retention profile (RP) data. Model parameters for specific partitioning scenarios were obtained through minimization of the objective function using the Gauss-Marquardt procedure (Marquardt, 1963):

$$O(\mathbf{b}) = \frac{1}{C_o^2}\sum_{i=1}^{N_a}\left[C_i - \hat{C}_i(\mathbf{b})\right]^2 + \sum_{i=1}^{N_s}\left\{w[Q_i - \hat{Q}_i(\mathbf{b})]\right\}^2 \quad (18)$$

where N_a and N_s are the number of effluent and in situ retention samples, $\mathbf{b}$ is the optimization parameter vector, w is a weighting factor to assign different weights to solid and aqueous concentrations, and the

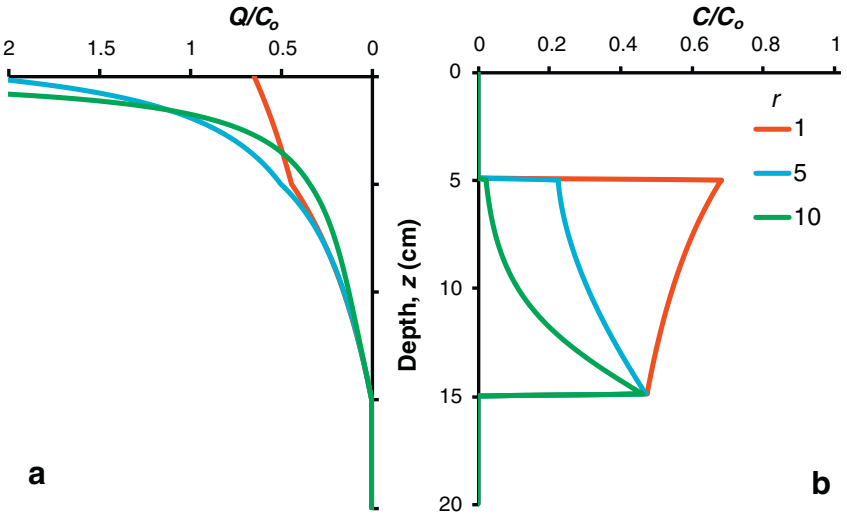

Fig. 4. Normalized solid (Q/C_o; Panel a) and aqueous (C/C_o; Panel b) phase concentrations versus depth at $t = 15$ min according to the ripening model for a pulse input with $C_o = 1$ cm^{-3}, $t_o = 10$ min, $V = 1$ cm/min, $k_a = 0.2$ min^{-1} with $r = 1$, 5, and 10 cm^3.

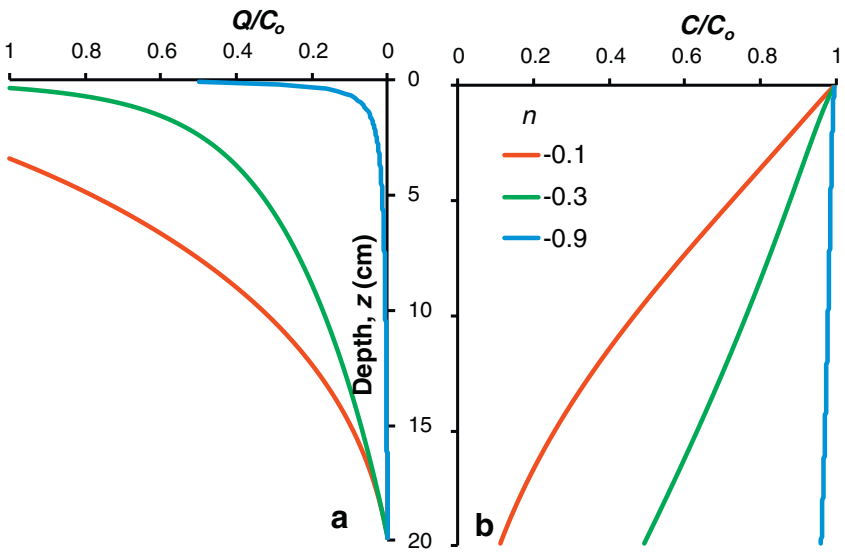

Fig. 5. Normalized solid (Q/C_o; Panel a) and aqueous (C/C_o; Panel b) phase concentrations versus depth at $t = 20$ min according to the depth-dependent model for a step input with $C_o = 1$ cm^{-3}, $V = 1$ cm/min, $k_a = 0.2$ min^{-1}, $k_d = 0.05$ min^{-1}, $d_{50} = 0.02$ cm, and three values for n: a) solid concentration (Q/C_o) and b) aqueous concentration (C/C_o).

caret denotes an optimized variable. Table 1 also contains optimized values as well as the coefficient of determination R^2 and root-mean square error. The latter is defined as:

$$RMSE = \sqrt{\frac{1}{(N-p)C_o^2}\left(\sum_{i=1}^{N_a}\left[C_i - \hat{C}_i(\mathbf{b})\right]^2 + \sum_{i=1}^{N_s}\left\{w\left[Q_i - \hat{Q}_i(\mathbf{b})\right]\right\}^2\right)} \quad (19)$$

where N is the total number of samples ($N = N_a + N_s$), and p is the number of optimized parameters.

4.1. Blocking

The analytical solution was used to describe effluent curves and retention profiles of *E. coli D21g* obtained by Wang et al. (2013). The effective diameter of *E. coli D21g* is 1.84 μm, which will potentially reduce retention because Q_m is inversely related to the square of colloid size (Bradford et al., 2013). A 30-min pulse of *E. coli D21g* was applied to an initially microbial-free sand column during steady water flow with an ionic strength of 20 mM. Fig. 8a shows observed effluent concentrations and Fig. 8b contains the retention profiles obtained by destructive sampling at the end of the displacement experiment. The relative high ionic strength diminishes repulsive forces between microbes and solid phase, which results in enhanced retention of *E. coli D21g*. Blocking causes the maximum retained concentration to be reached gradually while the effluent concentration keeps on increasing at a relatively rapid rate between 20 and 40 min. Hence Eqs. (7) and (8) were used to describe the data by optimizing k_a, k_d, and Q_m in blocking model (6). For comparison, the first-order model given by Eq. (3) was also fitted to the data. Fig. 8 includes optimized curves as well. The observations are better described with the reversible blocking than the first-order model although including a dispersion term could have further improved the description.

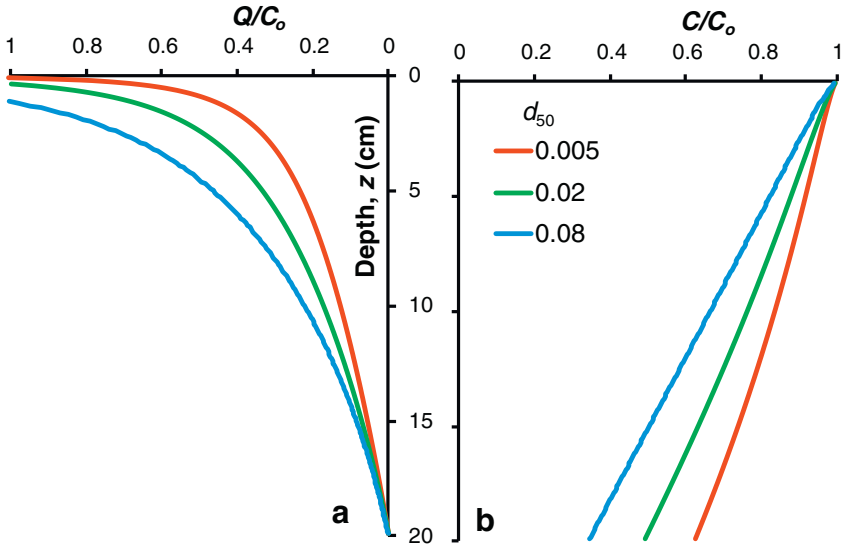

Fig. 6. Normalized solid (Q/C_o; Panel a) and aqueous (C/C_o; Panel b) phase concentrations versus depth at $t = 20$ min according to the depth-dependent model for a step input with $C_o = 1$ cm^{-3}, $V = 1$ cm/min, $k_a = 0.2$ min^{-1}, $k_d = 0.05$ min^{-1}, $n = -0.3$, and three values for d_{50}: a) solid concentration (Q/C_o) and b) aqueous concentration (C/C_o).

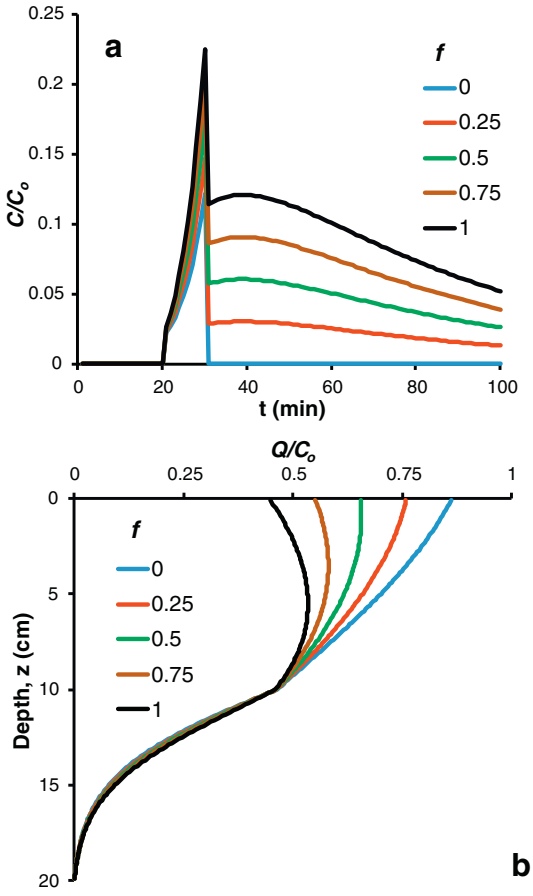

Fig. 7. Normalized solid (Q/C_o; Panel a) and aqueous (C/C_o; Panel b) phase concentrations versus depth at 20 min according to the blocking model with reversible and irreversible sites for a pulse input with $t_o = 10$ min, $k_a = 0.2$ min^{-1}, $k_d = 0.05$ min^{-1}, $V = 1$ cm/min, $Q_m = C_o = 1$ for five different fractions f of reversible sites (type 1).

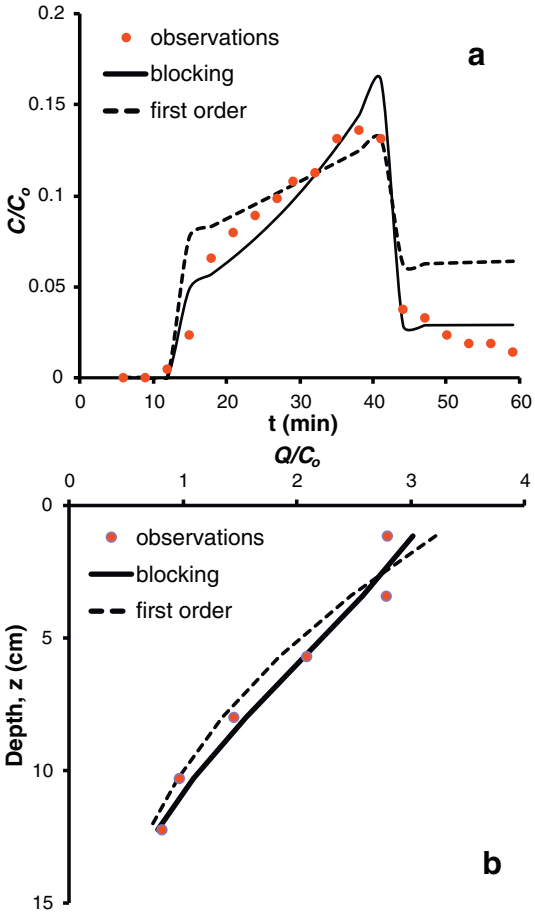

Fig. 8. Observed *E. coli D21g* concentrations at 20 mM ionic strength (Wang et al., 2013) and modeled profiles using reversible blocking or first-order partitioning as a function of (a) time and (b) depth.

4.2. Ripening

Kim et al. (2010) studied transport of *E. coli O157:H7* in ultra-pure quartz sand with an average diameter, d_{50}, of 275 μm in a 10-cm-long, 1.5-cm-diameter columns. A 184-min pulse of circa 5×10^8 cells/mL was applied in the form of KCl solutions. Data for an ionic strength of 0.01 mM were selected for optimization. The observed breakthrough data in Fig. 9 show that the maximum effluent concentration is reached after about 70 min. Subsequently the effluent concentration gradually decreases well before the entire pulse has passed through the sand column. This gradual decrease in aqueous concentration while colloid is still being applied is likely due to increased retention caused by

Table 1
Experimental and optimized parameters for four column studies shown in Figs. 8–11.

	Figure								
	8	9	10				11		
Partitioning model	Blocking	Ripening	Depth-dependent				Irreversible blocking		
Reference	Wang et al. (2013)	Kim et al. (2010a)	Kasel et al. (2013)				Sasidharan et al. (2014)		
Colloid	*E. coli D21g*	*E. coli O157:H7*	Multi-walled carbon nanotubes (MWNCT)				Latex nanoparticle		
V (cm/min)	0.95	0.217	1.51				6.94×10^{-2}		
t_o (min)	30	203	18.5				13.3×10^3		
L (cm)	13	10	12				11		
t_{exp} (min)	59.1	706	38.9				14.4×10^3		
θ	0.36	0.46	0.41				0.44		
Data	BTC, RP ($w = 0.2$)	BTC	BTC unimodal	RP	BTC, RP ($w = 0.1$) Bimodal type 1	($f = 0.5$) type 2	BTC Unimodal	Bimodal type 1	($f = 0.45$) type 2
k_a (min^{-1})	0.225	5.85×10^{-3}	0.549	2.92	0.392	∞	1.31×10^{-2}	1.25×10^{-2}	4.49×10^{-2}
k_d (min^{-1})	3.65×10^{-3}	1.2×10^{-3}	7.04×10^{-3}	0	1.19	5.93	–	–	–
	$Q_m/C_o = 5.04$	$r = 1.10$ cm^3	$n = -0.424$	$n = -0.437$	$n = -0.455$	$n = -1.05$	$Q_m/C_o = 75.6$	$Q_m/C_o = 24.8$	$Q_m/C_o = 263$
R^2	0.987	0.947	0.900	0.997	0.935		0.738	0.982	
RMSE ($\times 10^3$)	19.0	70.6	75	191	67.5		97.1	25.2	

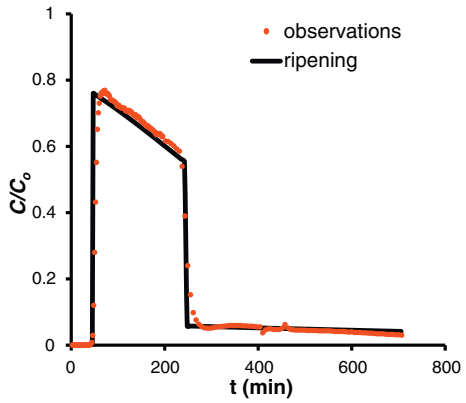

Fig. 9. Observed *E. coli O157:H7* breakthrough concentrations at 0.01 mM ionic strength (Kim et al., 2010) and modeled profiles using (unimodal) reversible ripening and (bimodal) reversible ripening and blocking.

ripening. The solution for the ripening model given by Eq. (12) is fitted to the effluent concentrations behavior yielding an R^2-value of 0.947.

4.3. Depth-dependent retention

The third data set involves transport of multi-walled carbon nanotubes (MWNCT) with a hydrodynamic radius of ranging between 170 and 210 nm (Kasel et al., 2013). A pulse of a 1 mM KCl-solution with 0.01 mg/L of radioactively ^{14}C-labeled MWCNT was applied to a 12-cm column packed with quartz sand with an average diameter of 607 μm. The experimental breakthrough curve and retention profiles are shown in Fig. 10. The retention data suggests that a depth-dependent model might be most appropriate for partitioning between aqueous and solid phases. The experimental breakthrough data exhibits some scatter, but a reasonable description of the data could be achieved with k_a, k_d, and n as optimization parameters and $d_{50} = 0.0607$ cm ($r^2 = 0.900$). The total mass in the effluent is slightly under predicted, perhaps due to experimental errors in V or t_o.

The retention data are well described with an irreversible model using k_a and n as optimization parameters with $k_d = 0$ and $d_{50} = 0.0607$ cm ($R^2 = 0.997$). No weighting of individual data points was employed to try to improve the fit for greater depths. Retention and breakthrough data were also optimized simultaneously using a two-site version of the depth-dependent model with a weight $w = 0.1$ for the retention profile. The initial estimates for the type-1 and type-2 parameters are based on the results for the one-site optimization of breakthrough and retention data, respectively. Type-2 values for all parameters were all quite large, but a fairly good description of the data could be obtained.

4.4. Irreversible blocking

The final data set is from the study by Sasidharan et al. (2014) on transport of 50-nm-latex microspheres in a 2 mM $CaCl_2$ solution. The solution was applied to an 11-cm-long column packed with natural graded river sand (average grain diameter of 255 μm) to establish a pore-water velocity of 1 m/d. The experimental data are shown in Fig. 11. Sasidharan et al. (2014) suggested that a two-site kinetic model is most appropriate to describe the data. The data were therefore modeled with a two-site and, for comparison, a one-site (unimodal) blocking function. Because detachment was found to be negligible, irreversible blocking functions were used. Fig. 11 and Table 1 indicate that a reasonably good description of the scattered data could be achieved with the two-site irreversible blocking function.

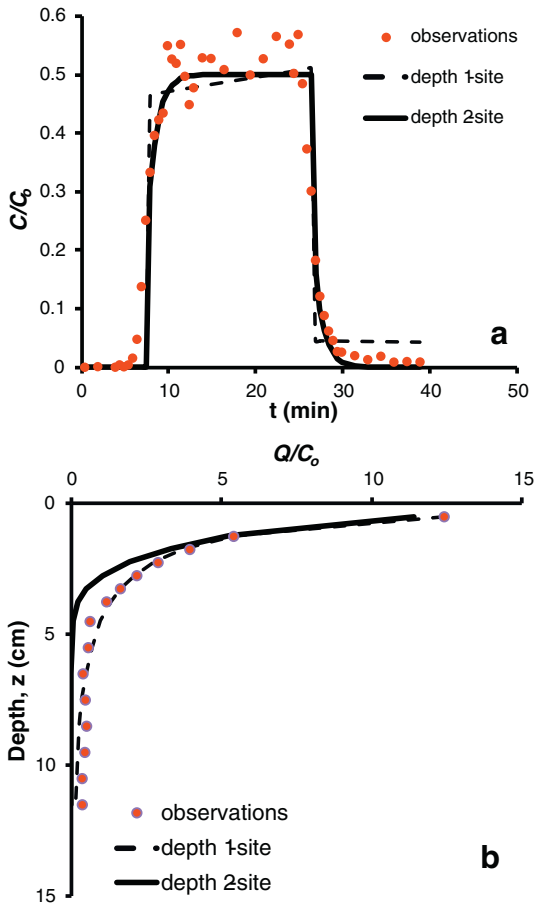

Fig. 10. Observed MWNCT concentrations (Kasel et al., 2013) and modeled profiles using separate (unimodal) and pooled (bimodal) depth-dependent retention as a function of (a) time and (b) depth.

5. Conclusions

Colloid transport and retention frequently exhibits complex time- and/or depth-dependent retention behavior. New analytical solutions for aqueous and solid phase colloid concentrations were derived to better understand and describe such behavior. In particular, the analytic solutions considered advective transport and a wide variety of reversible partitioning models, including: (1) first-order kinetics, (2) time-dependent blocking of retention sites, (3) time-dependent ripening of retention sites, and (4) depth-dependent retention. A bimodal model was also used with a different partitioning for two types of retention sites.

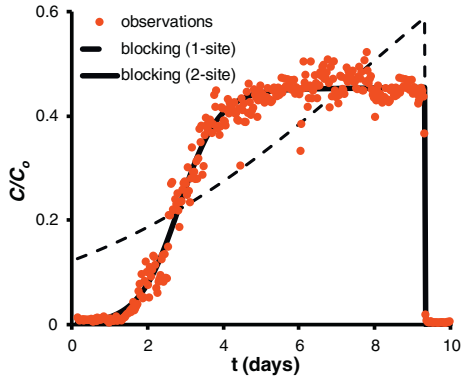

Fig. 11. Observed nanoparticle breakthrough concentrations at 2 mM ionic strength (Sasidharan et al., 2014) and predicted BTCs with uni- or bimodal irreversible blocking.

The developed solutions were subsequently used to illustrate the importance of partitioning model parameters and to analyze results from published experimental studies. The reversible blocking model demonstrated many observed complexities associated with colloid transport and retention such as increased effluent concentrations with continued colloid application, a delay in breakthrough, low concentration tailing, and retention profiles that are exponential, non-monotonic, or linear with distance. The ripening model can be used to account for a decrease in effluent concentration with continued colloid application and hyperexponential retention profiles. The depth-dependent retention model, which is a function of d_{50}, k_a, and an empirical parameter n, can also be used to describe time-invariant breakthrough curves and hyperexponential retention profiles. The two-site model conveniently allows the combination of the blocking, ripening, and depth-dependent partitioning models. The analytic solutions may also be used to verify numerical model results and to more conveniently simulate transport behavior at larger temporal and/or spatial scales than is possible with numerical models.

Acknowledgement

We would like to acknowledge and thank Kim et al. (2010), Kasel et al. (2013), Wang et al. (2013), and Sasidharan et al. (2014) for sharing their data.

Appendix A. Mathematical solution for blocking

The following variables are defined:

$$\xi = z/V \quad , \quad \tau = t - z/V \tag{A1a, b}$$

where Q is the solid concentration expressed as amount of colloids per volume of aqueous phase. The mathematical problem given by Eqs. (1)–(4) is transformed into:

$$\frac{\partial C}{\partial \xi} + \frac{\partial Q}{\partial \tau} = 0 \tag{A2}$$

$$\frac{\partial Q}{\partial \tau} = k_a \frac{Q_m - Q}{Q_m} C - k_d Q \tag{A3}$$

subject to the boundary and initial conditions:

$$C(0,\tau) = C_o H(t_o - \tau) \quad , \quad Q(\xi, 0) = 0 \tag{A4a, b}$$

with C_o as specified influent concentration and H as the Heaviside unit-step function. The conditions stipulate a pulse-type concentration at the inlet (where $\tau = t$) and a zero solid concentration ahead of the invading solution (when $\tau \le 0$). Because the problem is nonlinear, the superposition principle cannot be used to obtain the solution for a pulse input for that of a step input. The solution approach by Thomas (1944) is adapted by applying the transformations:

$$C = \frac{k_a}{Q_m}\left(\frac{1}{u}\frac{\partial u}{\partial \tau} - k_d\right) \tag{A5}$$

$$Q = -\frac{k_a}{Q_m}\left(\frac{1}{u}\frac{\partial u}{\partial \xi} - k_a\right) \tag{A6}$$

to rewrite (A3) as:

$$\frac{\partial^2 u}{\partial \xi \partial \tau} - k_a k_d u = 0 \tag{A7}$$

where $u(\xi,\tau)$ is an auxiliary function. The mathematical conditions on u are obtained by integrating Eqs. (A5) and (A6) with respect to τ and ξ while setting integration constants equal to unity (Thomas, 1944; Wade et al., 1987). The following conditions are obtained

$$u(0,\tau) = H(t_o - \tau)\exp(\beta\tau) + H(\tau - t_o)\exp(k_d\tau + \gamma t_o) \tag{A8}$$

$$u(\xi, 0) = \exp(k_a \xi) \tag{A9}$$

where β and γ are given by Eqs. (11a, b, c). Eq. (A7) is a linear hyperbolic equation that may be solved by Riemann's method (Thomas, 1944; Zwillinger, 1997). Wade et al. (1987) solved the problem with a double Laplace transform. Here a simpler single Laplace transformation will be used with respect to ξ, i.e.:

$$U(\xi, p) = L\{u(\xi,\tau)\} = \int_0^\infty u(\xi,\tau)\exp(-p\tau)d\tau \tag{A9}$$

with p as the Laplace variable. The problem in the Laplace domain becomes:

$$p\frac{dU}{d\xi} - k_a \exp(k_a x) = k_a k_d U \tag{A10}$$

subject to the boundary condition

$$U(0,p) = \frac{1}{p-\beta} - \exp[-(p-\beta)t_o]\left(\frac{1}{p-\beta} - \frac{1}{p-k_d}\right) \tag{A11}$$

The following solution of Eq. (A10) may be obtained using the method of undetermined coefficients or mathematical software:

$$U(\xi,\tau) = \{1 - \exp[-(p-\beta)t_o]\}\left(\frac{1}{p-\beta} - \frac{1}{p-k_d}\right)\exp\left(\frac{k_a k_d \xi}{p}\right) + \frac{\exp(k_a\xi)}{p-k_d} \tag{A12}$$

The inversion can be done with the inversion pairs:

$$L^{-1}\left\{\frac{\exp(b/p)}{p-a}\right\} = \exp(ay + b/a)J(b/a, a\tau) \tag{A13}$$

$$L^{-1}\left\{\frac{\exp(-cp + b/p)}{p-a}\right\} = H(\tau - c)\exp[a(y-c) + b/a]J(b/a, a(\tau - c)) \tag{A14}$$

where the J-function by Goldstein (1953) is defined as:

$$J(a,b) = \exp(-a)[1 + \int_0^b \sqrt{\frac{a}{\lambda}}\exp(-\lambda)I_1\left(2\sqrt{a\lambda}\right)d\lambda] \tag{A15a}$$

$$J(b,a) = 1 - \exp(-a)\int_0^b \exp(-\lambda)I_0\left(2\sqrt{a\lambda}\right)d\lambda \tag{A15b}$$

where I_0 and I_1 are the zero-and first-order modified Bessel function of the first kind. Various approximations for the J-function have been published (Goldstein, 1953; van Genuchten, 1981). After inversion the solution for the auxiliary function becomes:

$$u(\xi,\tau) = \exp(\alpha\xi + \beta\tau)[J(\alpha\xi, \beta\tau) - H(\tau - t_o)J(\alpha\xi, \beta(\tau - t_o))] + \exp(k_a\xi + k_d\tau)[1 - J(k_a\xi, k_d\tau) + H(\tau - t_o)\exp(\gamma t_o)J(k_a\xi, k_d(\tau - t_o))] \tag{A16}$$

The aqueous and solid concentrations are obtained from u according to Eqs. (A5) and (A6). First-order derivatives follow from Eq. (A15), i.e.:

$$\frac{\partial J(a,b)}{\partial a} = -\exp(-a-b)I_0\left(2\sqrt{ab}\right) \tag{A17a}$$

$$\frac{\partial J(a,b)}{\partial b} = \exp(-a-b)\sqrt{\frac{a}{b}}I_1\left(2\sqrt{ab}\right) \tag{A17b}$$

The following identity is used to improve the evaluation of the Goldstein function:

$$\exp(a+b)J(a,b) = \exp(a+b)-\int_0^a \exp(a-\lambda)I_0\left(2\sqrt{\lambda b}\right)d\lambda = \exp(a+b)-\Gamma(a,b) \tag{A18}$$

where the auxiliary function Γ is determined by numerical integration using Gauss-Chebyshev quadrature. The solutions (4) and (5) are written in terms of regular independent variables z and t by invoking Eq. (A1a, b).

Appendix B. Mathematical solution for spatially dependent retention

The mathematical problem for the second-type of reversible, spatially dependent retention according to Hosseini and Tosco (2013) is given by:

$$\frac{\partial C}{\partial t}+\frac{\partial Q}{\partial t}+V\frac{\partial C}{\partial z}=0 \tag{B1}$$

$$\frac{\partial Q}{\partial t}=k_a\left(1+\frac{z}{d_{50}}\right)^n C-k_d Q \tag{B2}$$

where α is the mean diameter of the porous material, and the exponent β quantifies the dynamics of retention. The boundary and initial conditions are again for a pulse application to an initially colloid-free medium:

$$C(0,t)=C_o H(t_o-t) \quad , \quad C(z,0)=Q(z,0)=0 \tag{B3a, b}$$

The problem is solved by applying the following Laplace transform

$$\overline{C}(z,s)=L\{C(z,t)\}=\int_0^\infty C(z,t)\exp(-st)dt \tag{B4}$$

with s as the Laplace variable corresponding to time. Combining the transformed results of Eqs. (B1) and (B2) and yields the following first-order ordinary differential equation:

$$\frac{d\overline{C}}{dz}+\frac{s}{V}\left[1+\frac{k_a(1+z/d_{50})^n}{s+k_d}\right]=0 \tag{B5}$$

subject to

$$\overline{C}(0,s)=\frac{C_o}{s}[1-\exp(-st_o)] \tag{B6}$$

Integration of Eq. (B5) and application of inlet condition (B6) yields the solution:

$$\overline{C}(z,s)=\frac{C_o}{s}[1-\exp(-st_o)]\exp\left(-\frac{zs}{V}-\frac{As}{s+k_d}\right) \quad , \tag{B7a, b}$$

$$A=\frac{d_{50}k_a}{(1+n)V}\left[\left(1+\frac{z}{d_{50}}\right)^{1+n}-1\right]$$

The following inversion pair is used

$$L^{-1}\left\{\frac{1}{s}\exp\left(\frac{m}{s+n}\right)\right\}=\exp\left(\frac{m}{n}\right)J\left(\frac{m}{n},nt\right) \tag{B8}$$

with the J-function (Goldstein, 1953) defined by Eq. (A15).

The solution for the aqueous phase becomes:

$$C(z,t)=C_o[J(A,k_d(t-z/V))-J(A,k_d(t-t_o-z/V))] \tag{B9}$$

The following Laplace transformation of Eq. (B2) is used to determine the solid concentration:

$$\overline{Q}(z,s)=\frac{k_a}{s+k_d}(1+z/\alpha)^\beta\overline{C}(z,s) \tag{B10}$$

Substitution of Eq. (B7a) gives:

$$\overline{Q}(z,s)=\frac{C_o}{s}\frac{k_a}{s+k_d}\left(1+\frac{z}{\alpha}\right)^\beta\exp(-A) \times\left[\exp\left(-\frac{zs}{V}\right)-\exp\left(-st_o-\frac{zs}{V}\right)\right]\exp\left(\frac{Ak_d}{s+k_d}\right) \tag{B11}$$

Using the inversion pair

$$L^{-1}\left\{\frac{1}{s}\frac{1}{s+k_d}\exp\left(\frac{a}{s+b}\right)\right\}=\frac{1}{b}\exp\left(\frac{a}{b}\right)\left[1-J\left(bt,\frac{a}{b}\right)\right] \tag{B12}$$

yields the expression for the solid concentration:

$$Q(z,t)=\frac{k_aC_o}{k_d}\left(1+\frac{z}{d_{50}}\right)^n\left[J\left(k_d\left(t-\frac{z}{V}\right),A\right)-J\left(k_d\left(t-t_o-\frac{z}{V}\right),A\right)\right] \tag{B13}$$

References

Adamczyk, Z., Siwek, B., Zembala, M., Belouschek, P., 1994. Kinetics of localized adsorption of colloid particles. Adv. Colloid Interface 48:151–280. http://dx.doi.org/10.1016/0001–8686(94)80008-1.

Bohart, G.S., Adam, E.Q., 1920. Some aspects of the behavior of charcoal with respect to chlorine. J. Am. Chem. Soc. 42, 523–529.

Boxall, A.B., Tiede, K., Chaudhry, Q., 2007. Engineered nanomaterials in soils and water: how do they behave and could they pose a risk to human health? Nanomedicine 2, 919–927.

Bradford, S.A., Torkzaban, S., 2015. Determining parameters and mechanisms of colloid retention and release in porous media. Langmuir 31 (44), 12096–12105.

Bradford, S.A., Simunek, J., Bettahar, M., van Genuchten, M.T., Yates, S.R., 2003. Modeling colloid attachment, straining, and exclusion in saturated porous media. Environ. Sci. Technol. 37, 2242–2250.

Bradford, S.A., Simunek, J., Walker, S.L., 2006. Transport and straining of *E. coli* O157: H7 in saturated porous media. Water Resour. Res. 42 (12). http://dx.doi.org/10.1029/2005WR004805.

Bradford, S.A., Torkzaban, S., Simunek, J., 2011. Modeling colloid transport and retention in saturated porous media under unfavorable attachment conditions. Water Resour. Res. 47 (10). http://dx.doi.org/10.1029/2011WR010812.

Bradford, S.A., Torkzaban, S., Shapiro, A., 2013. A theoretical analysis of colloid attachment and straining in chemically heterogeneous porous media. Langmuir 29, 2952–6944.

Camesano, T.A., Unice, K.M., Logan, B.E., 1999. Blocking and ripening of colloids in porous media and their implications for bacterial transport. Colloids Surf. A Physicochem. Eng. Asp. 160, 291–308.

Chowdhury, I., Hong, Y., Honda, R.J., Walker, S.L., 2011. Mechanisms of TiO2 nanoparticle transport in porous media: role of solution chemistry, nanoparticle concentration, and flowrate. J. Colloid Interface Sci. 360, 548–555.

Chu, K.H., 2010. Fixed bed sorption: Setting the record straight on the Bohart–Adams and Thomas models. J. Hazard. Mater. 177, 1006–1012.

Deshpande, P.A., Shonnard, D.R., 1999. Modeling the effects of systematic variation in ionic strength on the attachment kinetics of *Pseudomonas fluorescens* UPER-1 in saturated sand columns. Water Resour. Res. 35, 1619–1627.

Gerba, C.P., Smith, J.E., 2005. Sources of pathogenic microorganisms and their fate during land application of wastes. J. Environ. Qual. 34 (1), 42–48.

Goldstein, S., 1953. On the mathematics of exchange processes in fixed columns I. Mathematical solutions and asymptotic expansions. Proc. R. Soc. London Ser. A 219, 151–185.

Harvey, R.W., Garabedian, S.P., 1991. Use of colloid filtration theory in modeling movement of bacteria through a contaminated sandy aquifer. Environ. Sci. Technol. 25 (1), 178–185.

Hiester, N.K., Vermeulen, T., 1952. Saturation performance of ion-exchange and adsorption columns. Chem. Eng. Prog. 48 (10), 505–516.

Hosseini, S.M., Tosco, T., 2013. Transport and retention of high concentrated nano-Fe/Cu particles through highly flow-rated packed sand column. Water Res. 47, 326–338.

Javandel, I., Doughty, C., Tsang, C.-F., 1984. Groundwater Transport: Handbook of Mathematical Models. Water Resour. Monograph no. 10. Am. Geophys. Union, Washington, D.C.

Kasel, D., Bradford, S.A., Simunek, J., Heggen, M., Vereecken, H., Klumpp, E., 2013. Transport and retention of multi-walled carbon nanotubes in saturated porous media: effects of input concentration and grain size. Water Res. 47, 933–944.

Kim, H.N., Walker, S.L., Bradford, S.A., 2010. Macromolecule mediated transport and retention of *Escherichia coli*O157: H7 in saturated porous media. Water Res. 44: 1082–1093. http://dx.doi.org/10.1016/j.watres.2009.09.027.

Lapidus, L., Amundson, N.R., 1952. Mathematics of adsorption in beds: VI the effect of longitudinal diffusion in ion exchange and chromatographic columns. J. Phys. Chem. 56, 984–988.

Leij, F.J., Sciortino, A., 2012. Solute transport. In: Huang, P.M., Li, Y., Sumner, M.E. (Eds.), Handbook of Soil Science, second ed. CRC Press Taylor & Francis Group, Boca Raton, FL.

Leij, F.J., Bradford, S.A., Wang, Y., Sciortino, A., 2015. Langmuirian blocking of irreversible colloid retention: analytical solution, moments, and setback distance. J. Environ. Qual. 44:1473–1482. http://dx.doi.org/10.2134/jeq2015.03.0147.

Li, X., Scheibe, T.D., Johnson, W.P., 2004. Apparent decreases in colloid deposition rate coefficients with distance of transport under unfavorable deposition conditions: A general phenomenon. Environ. Sci. Technol. 38 (21), 5616–5625.

Liang, Y., Bradford, S.A., Simunek, J., Vereecken, H., Klumpp, E., 2013. Sensitivity of the transport and retention of stabilized silver nanoparticles to physicochemical factors. Water Res. 47, 2572–2582.

Mao, J., Kim, S., Wu, X.H., Kwak, I.-S., Zhou, T., Yun, Y.-S., 2015. A sustainable cationic chitosan/*E. coli* fiber biosorbent for Pt(IV) removal and recovery in batch and column systems. Sep. Purif. Technol. 143, 32–39.

Marquardt, D.W., 1963. An algorithm for least-squares estimation of non-linear parameters. J. Soc. Ind. Appl. Math. 11, 431–441.

Neukum, C., Braun, A., Azzam, R., 2014. Transport of stabilized engineered silver (Ag) nanoparticles through porous sandstones. J. Contam. Hydrol. 158, 1–13.

Ryan, J.N., Elimelech, M., 1996. Colloid mobilization and transport in groundwater. Colloids Surf. A Physicochem. Eng. Asp. 107, 1–56.

Sasidharan, S., Torkzaban, S., Bradford, S.A., Dillon, P.J., Cook, P.G., 2014. Coupled effects of hydrodynamic and solution chemistry on long-term nanoparticle transport and deposition in saturated porous media. Colloids Surf. A Physicochem. Eng. Asp. 457, 169–179.

Sen, T.K., Khilar, K.C., 2006. Review on subsurface colloids and colloid-associated contaminant transport in saturated porous media. Adv. Colloid Interf. Sci. 119 (2), 71–96.

Sposito, G., 1989. The Chemistry of Soils. Oxford University Press, New York.

Thomas, H.C., 1944. Heterogeneous ion exchange in a flowing system. J. Am. Chem. Soc. 66, 1664–1666.

Thomas, H.C., 1948. Chromatography: a problem in kinetics. Ann. N. Y. Acad. Sci. 49, 161–182.

Tong, M., Li, X., Brow, C.N., Johnson, W.P., 2005. Detachment-influenced transport of an adhesion-deficient bacterial strain within water-reactive porous media. Environ. Sci. Technol. 39 (8), 2500–2508.

Torkzaban, S., Bradford, S.A., Vanderzalm, J.L., Patterson, B.M., Harris, B., Prommer, H., 2015. Colloid release and clogging in porous media: effects of solution ionic strength and flow velocity. J. Contam. Hydrol. 181, 161–171.

Tufenkji, N., Elimelech, M., 2005. Breakdown of colloid filtration theory: role of the secondary energy minimum and surface charge heterogeneities. Langmuir 21 (3), 841–852.

van Genuchten, M.T., 1981. Non-equilibrium transport parameters from miscible displacement experiments. Research Report 119. U.S. Salinity Laboratory, USDA, ARS, Riverside, CA.

Vanderborght, J., Kasteel, R., Herbst, M., Javaux, M., Thiéry, D., Vanclooster, M., Mouvet, C., Vereecken, H., 2005. A set of analytical benchmarks to test numerical models of flow and transport in soils. Vadose Zone J. 4, 206–221.

Vijayaraghavan, K., Yun, Y.-S., 2008. Bacterial biosorbents and biosorption. Biotechnol. Adv. 26, 266–291.

Wade, J.L., Bergold, A.F., Carr, P.W., 1987. Theoretical description of nonlinear chromatography, with applications to physicochemical measurements in affinity chromatography and implications for preparative-scale separations. Anal. Chem. 59, 1286–1295.

Wang, Y., Bradford, S.A., Simunek, J., 2013. Transport and fate of microorganisms in soils with preferential flow under different solution chemistry conditions. Water Resour. Res. 49:2424–2436. http://dx.doi.org/10.1002/wrcr.20174.

Yao, K., Habibian, M.T., O'Melia, C.R., 1971. Water and wastewater filtration concepts and applications. Environ. Sci. Technol. 5 (11), 1105–1112.

Yuan, H., Shapiro, A.A., 2012. Colloid transport and retention: recent advances in colloids filtration theory. In: Ray, P.C. (Ed.), Colloids: Classification, Properties, and Applications. 9:201–241. Nova Science Publishers, Inc.

Zwillinger, D., 1997. Handbook of Differential Equations. Academic Press, San Diego.